doi:10.1093/brain/aww271 BRAIN 2017: 140; 201–217 | 201

BRAIN
A JOURNAL OF NEUROLOGY

The chemokine CXCL12 mediates the anti-amyloidogenic action of painless human nerve growth factor

Simona Capsoni,[1,2,*] Francesca Malerba,[1,3] Nicola Maria Carucci,[1] Caterina Rizzi,[1] Chiara Criscuolo,[2,4] Nicola Origlia,[2] Mariantonietta Calvello,[1] Alessandro Viegi,[1] Giovanni Meli[3] and Antonino Cattaneo[1,3]

Nerve growth factor is a therapeutic candidate for Alzheimer's disease. Due to its pain-inducing activity, in current clinical trials nerve growth factor is delivered locally into the brain by neurosurgery, but data on the efficacy of local nerve growth factor delivery in decreasing amyloid-β deposition are not available. To reduce the nerve growth factor pain-inducing side effects, thus avoiding the need for local brain injection, we developed human painless nerve growth factor (hNGFp), inspired by the human genetic disease hereditary sensory and autonomic neuropathy type V. hNGFp has identical neurotrophic potency as wild-type human nerve growth factor, but a 10-fold lower pain sensitizing activity. In this study we first mimicked, in the 5xFAD mouse model, the intraparenchymal delivery of hNGFp used in clinical trials and found it to be ineffective in decreasing amyloid-β plaque load. On the contrary, the same dose of hNGFp delivered intranasally, which was widely biodistributed in the brain and did not induce pain, showed a potent anti-amyloidogenic action and rescued synaptic plasticity and memory deficits. We found that hNGFp acts on glial cells, modulating inflammatory proteins such as the soluble TNFα receptor II and the chemokine CXCL12. We further established that the rescuing effect by hNGFp is mediated by CXCL12, as pharmacological inhibition of CXCL12 receptor CXCR4 occludes most of hNGFp effects. These findings have significant therapeutic implications: (i) we established that a widespread exposure of the brain is required for nerve growth factor to fully exert its neuroprotective actions; and (ii) we have identified a new anti-neurodegenerative pathway as a broad target for new therapeutic opportunities for neurodegenerative diseases.

1 Bio@SNS Laboratory of Biology, Scuola Normale Superiore, Pisa, Italy
2 Institute of Neuroscience, National Council for Research, Pisa, Italy
3 Neurotrophins and Neurodegenerative Diseases Laboratory, Rita Levi-Montalcini European Brain Research Institute, Rome, Italy
4 Department of Biotechnological and Applied Clinical Sciences, School of Medicine, University of L'Aquila, Coppito, L'Aquila, Italy

*Present address: Department of Medical Biomedical and Specialty Surgical Sciences, University of Ferrara, Italy

Correspondence to: Prof. Antonino Cattaneo,
BIO@SNS Laboratory of Biology, Scuola Normale Superiore, Piazza dei Cavalieri 7, Pisa, Italy
E-mail: antonino.cattaneo@sns.it

Keywords: Alzheimer; nerve growth factor; intranasal; CXCL12; pain

Abbreviations: BFCN = basal forebrain cholinergic neuron; hNGFp = human painless nerve growth factor; NBM = nucleus basalis of Meynert

Received June 7, 2016. Revised August 19, 2016. Accepted September 7, 2016

Introduction

A selective vulnerability of basal forebrain cholinergic neurons (BFCNs) contributes to cognitive decline in Alzheimer's disease patients (Bartus *et al.*, 1982; Whitehouse *et al.*, 1982). BFCNs depend on the neurotrophin nerve growth factor (NGF) (Levi-Montalcini, 1952) for their maintenance and survival (Mufson *et al.*, 1999). For this reason, the clinical application of NGF for Alzheimer's disease is being pursued. However, due to the poor biodistribution of NGF to the brain after systemic delivery (Poduslo and Curran, 1996) and to its potent pro-nociceptive activity after systemic (Petty *et al.*, 1994) and intrathecal (Malcangio *et al.*, 2000) administration, current clinical trials are based on the neurosurgical injection close to the nucleus basalis of Meynert (NBM) of NGF-secreting cells or of vectors carrying the *NGF* gene (Tuszynski *et al.*, 2005; Mandel, 2010; Eriksdotter-Jonhagen *et al.*, 2012). These trials report a positive effect on BFCNs and on cognition, but the outcome on Alzheimer's disease hallmarks such as amyloid pathology were not described in patients (Tuszynski *et al.*, 2005; Mandel, 2010; Eriksdotter-Jonhagen *et al.*, 2012; Ferreira *et al.*, 2015; Karami *et al.*, 2015). In preclinical testing, after 3 months local infusion of NGF in non-human primate brains, amyloid-β deposition was found to be identical as in age-matched controls (Tuszynski *et al.*, 1998).

To reduce the pain-inducing side effects of NGF, we developed painless NGF (hNGFp), a double mutant form of NGF (hNGFP61S/R100E) inspired by the human genetic disease hereditary sensory and autonomic neuropathy type V (HSAN V) (Einarsdottir *et al.*, 2004). hNGFp harbours the mutation R100E, to reduce the pro-nociceptive activity of NGF (Covaceuszach *et al.*, 2009; Capsoni *et al.*, 2012; Malerba *et al.*, 2015) and a second mutation (P61S), allowing its specific immunodetection against endogenous NGF. hNGFp is a TrkA biased agonist, in that it effectively binds and activates TrkA, although with a different signalling profile, while its binding affinity to p75NTR is strongly reduced (Covaceuszach *et al.*, 2010; Capsoni *et al.*, 2012). hNGFp has identical neurotrophic potency as wild-type human NGF (hNGF), but a 10-fold lower pain sensitizing activity (Capsoni *et al.*, 2012; Malerba *et al.*, 2015) and thus a broader therapeutic window.

In this paper, we studied the efficacy of hNGFp in counteracting neurodegeneration and behavioural deficits in the aggressive mouse model 5xFAD (Oakley *et al.*, 2006), starting the treatment at an age when the pathology is already evident. First, we mimicked the intraparenchymal route currently used in clinical trials and, surprisingly, we found no effect of hNGFp on amyloid-β deposition. Thus, we switched to the intranasal delivery, a non-invasive method to convey neurotrophic factors to the brain (Frey *et al.*, 1997) at pharmacologically and therapeutically relevant doses (Capsoni *et al.*, 2002*b*, 2009, 2012; De Rosa *et al.*, 2005).

We found that, contrary to the intraparenchymal administration, the intranasal delivery of hNGFp determines the rescue of synaptic plasticity, memory deficits and neurodegeneration in 5xFAD mice, with a significant reduction of amyloid-β amyloid deposition. These actions are mediated by glial cells, via the direct involvement of the CXCL12 chemokine. Overall, these data support the emerging concept that the neuroprotective actions of NGF in the brain go well beyond BFCNs (Levi-Montalcini *et al.*, 1996; Capsoni and Cattaneo, 2006; Cattaneo *et al.*, 2008; Capsoni *et al.*, 2011; Cattaneo and Calissano, 2012) and demonstrate glial cells and chemokines as a broad target for hNGFp actions in the brain, with significant clinical and therapeutic implications.

Materials and methods

Study design

This study explored the efficacy of two methods of delivery of a mutant form of NGF in decreasing amyloid-β deposition in a mouse model overexpressing mutant human APP and presenilin 1. All experiments were conducted according to the ARRIVE guidelines (Animal Research: Reporting *In Vivo* Experiments). Animals were randomized and coded so that the persons carrying out behavioural analysis and tissue processing, and statistical analysis were blind to the treatment. Randomization was carried out using the Research Randomizer Program online (www.randomizer.org). The GPower program was used to calculate *a priori* the sample size. Power, alpha and effect size were set at 80%, 0.05 and 0.25, respectively. A one-way ANOVA test followed by a Tukey HSD test was performed based on published data on the Y-maze test (Kimura *et al.*, 2010).

Transgenic mice

Transgenic mice with five familial Alzheimer's disease mutations (5xFAD) were purchased from The Jackson Laboratory. 5xFAD transgenic mice that co-overexpress FAD mutant forms of human APP (the Swedish mutation: K670N, M671L; the Florida mutation: I716V; the London mutation: V717I) and presenilin 1 (PS1, encoded by *Psen1*: M146L, L286V) transgenes under transcriptional control of the neuron-specific mouse *Thy1* promoter (Oakley *et al.*, 2006). 5xFAD mice used were hemizygotes with respect to the transgenes and non-transgenic wild-type littermates were used as controls. Genotyping was performed by PCR analysis of tail DNA. All analyses were done blind with respect to the genotype of the mice and treatment. The number of subjects in the experiments are reported in the figure legends. All experiments with mice were performed according to the national and international laws for laboratory animal welfare and experimentation (EU directive n. 2010/63/EU and Italian DL n. 26 04/03/2014). Mice were kept under a 12-h dark to light cycle, with food and water *ad libitum*.

Human tissues

Tissues from parietal cortex from three Alzheimer's disease patients and three control subjects were obtained from The Netherlands Brain Bank (Amsterdam, The Netherlands) and from the Policlinico Tor Vergata (Rome, Italy), respectively. All patients were clinically diagnosed for absence or presence of Alzheimer's disease (Supplementary Table 3). For immunohistochemistry, frozen samples were fixed in 4% paraformaldehyde and stored in 20% sucrose plus 0.05% sodium azide until use. Samples were then sectioned at 20 µm, collected on SuperFrost® microscope slides (Sigma-Aldrich) and processed for immunohistochemistry as described below.

Human NGF mutant expression and purification

hNGF and hNGFp expression and purification was performed as previously described (Covaceuszach *et al.*, 2009; Malerba *et al.*, 2015). Briefly, hNGF mutants were expressed in *Escherichia coli* as unprocessed proNGF, refolded *in vitro* from inclusion bodies, and mature NGF was obtained from *in vitro*-refolded proNGF by controlled proteolysis, followed by chromatograph. Human BDNF (hBDNF) was obtained from Alomone Labs.

Treatments

Intranasal treatment with human painless NGF or human BDNF

hNGF and hNGFp were administered intranasally at the doses of 0.27, 0.54, 1.08, 2.7 and 5.4 µg/kg (equivalent to 0.26, 0.51, 1.04, 2.6 and 5.6 pmol). hBDNF was administered at the dose of 54 µg/kg (equivalent to 48.56 pmol). The peptides were diluted in 1 M phosphate-buffered saline (PBS, 137 mM NaCl, 2.7 mM KCl, 10 mM Na_2HPO_4, 1.8 mM K_2HPO_4 pH 7.4) and administered intranasally to mice, 3 µl at a time, alternating the nostrils, with a lapse of 2 min between each administration, for a total of 14 times. During these procedures, the nostrils were always kept open. As control treatments, wild-type and 5xFAD mice were treated with PBS. The frequency of administration for intranasal delivery was three times per week (every 2 days). Administrations were repeated nine times, over a 21-day period, followed by 7 days of washout during which mice were not dosed with the proteins. For acute, single administration used to determine the biodistribution of hNGFp, due to the limits of sensitivity of the ELISA assay, wild-type mice were administered with 10 µg/kg of hNGFp.

Intraparenchymal administration of human painless NGF

Dosing to the NBM was achieved using Alzet osmotic minipumps (Charles River), which allowed the continuous administration of hNGFp over a period of 28 days. The daily dose was equivalent to the intranasal dose: 0.54 µg/kg. Control animals were represented by 5xFAD mice implanted with a mini-osmotic pump releasing PBS. The mini-osmotic pumps were prepared according to the manufacturer's instructions. On the day of surgery, mice were anaesthetized with 10 µl/g of body weight of a 2.5% solution of 2,2,2-tribromethanol (Sigma-Aldrich). Minipumps were implanted into the brain in proximity of the NBM according to the following coordinates: bregma: −0.6 mm, lateral to sagittal suture: 2.1 mm, depth: 3.5 mm.

Co-administration of human painless NGF and the CXCR4 inhibitor AMD3100

hNGFp was administered at the dose of 0.54 µg/kg, according to the scheme described above. The CXCR4 AMD3100 inhibitor was administered subcutaneously at a dose of 1 mg/kg twice a day to mice that were treated intranasally with PBS or hNGFp. Due to the pharmacokinetic effect of AMD3100, mice were treated over a period of 20 days and immediately tested to assess the effects on behaviour, and sacrificed.

Orofacial stimulation test

Hypersensitivity to mechanical stimulation of the trigeminal area was tested using the orofacial stimulation apparatus (Ugo Basile). Male wild-type and 5xFAD mice were tested in standard rat cages. Mice were freely allowed to insert the snout through an opening to lick the reward bottle containing sweetened milk. Tests were performed in the presence of a mechanical stimulus contacting the vibrissal pad. The mechanical stimulator relied on thin wires attached to a black mounting plate. Feeding duration and number of attempts are strongly dependent on changes in the applied mechanical stimulus or to hypersensitivity to stimuli. The duration of feeding was obtained by automatically measuring the interruption of an infrared barrier traversing the opening to the reward. Records were processed and graphically represented using the ORO software (Ugo Basile).

Y-maze test

Spatial working memory performance was assessed using the Y-maze test, as described previously (Maurice *et al.*, 1998). The maze was made of dark grey wood and constituted three arms. Each arm was 40 cm long, 13 cm high and 10 cm wide and converged at an equal angle. Each male mouse was placed at the end of one arm and allowed to move freely through the maze during an 8-min session. The series of arm entries, including the possible returns in the same arm, was recorded. An alternation was defined as entries into the three arms on consecutive events. The number of maximum alternations was equal to the total number of entries minus two. The percentage of spontaneous alternations (%SAP) was calculated according the following formula: %SAP = number of alternations/maximum entries × 100.

Peripheral mechanical allodynia

The experiment was performed as described previously (Capsoni *et al.*, 2012), using as positive control an intraplantar injection of hNGF at the dose of 4 µl/animal. Measurements were taken 1 and 3 h post-injection.

Electrophysiological recordings

Entorhinal cortex slices preparation

Entorhinal cortex slices were prepared according to the procedure previously described (Pesavento *et al.*, 2002). Animals were deeply anaesthetized (20% urethane solution, 0.1 ml/100 g body weight) via intraperitoneal injection and decapitated after tail pinch reflex disappearance in order to perform the immediate dissection of brain tissue. Horizontal slices containing entorhinal area (400-µm thick) were obtained by a vibratome (Leica VT1200S). All of the above steps were performed in ice-cold artificial CSF solution (in mM: NaCl, 119; KCl, 2.5; $CaCl_2$, 2; $MgSO_4$, 1.2; NaH_2PO_4, 1; $NaHCO_3$, 26.2; glucose, 10) bubbled with 95% O_2/5% CO_2. Slices were stored in a recovery chamber containing oxygenated artificial CSF solution at room temperature, for at least 1 h prior to electrophysiological recording. At recording time, the single slice was transferred to a chamber, where it was perfused at constant flow (2 ml/min) with oxygenated artificial CSF, at 33 ± 1°C.

Electrophysiological recordings

Extracellular field potentials were evoked via a bipolar tungsten electrode placed in cortical layer II, while the recording electrode (pulled glass capillaries, outer diameter = 1.0 mm, inner diameter = 0.78 mm) was placed in cortical layer II/III. The amplitude of the negative deflection of the field potential was used as a measure of the population of the excitatory currents that are evoked by the stimulus (Origlia *et al.*, 2008). The stimulus was applied through an insulator (Digitimer DS2A) and base recording condition was carried out by an intensity capable of evoking a response with an amplitude of between 50 and 60% of the maximum response. Amplitudes of field potentials were calculated at different stimulus intensities to obtain input-output curves. All field potentials had peak latency between 4.5 to 6 ms. The signal was amplified and filtered (WPI, DAM 80) and field potential amplitudes were monitored every 20 s and averaged every three responses by online data acquisition software (Anderson and Collingridge, 2001). Experiments to assess paired-pulse stimulation (PP) were also performed: two consecutive stimuli were applied at different interstimulus intervals (25–200 ms). PP-induced change was calculated as the ratio of the peak amplitude of the second field potential to the first one. After 15 min of stable baseline, long-term potentiation (LTP) was induced, recording high frequency stimulation (HFS, three trains of 100 pulses at 100 Hz, 10 s interval). After HFS, field potentials continued to be monitored every 20 s for at least 50 min. The magnitude of LTP was calculated as the average of the relative amplitudes (compared to baseline) of field potentials recorded in the last 10 min of recording protocol. Values were expressed as mean ± standard error of the mean (SEM) percentage change relative to their mean baseline amplitude. Acute applications of hNGFp (100 ng/ml) on entorhinal cortex slices were performed through general perfusion for 10 min starting 5 min before HFS. The tyrosine kinase inhibitor K252a (200 nM; Sigma Aldrich) was applied through general perfusion for 20 min starting from 15 min before HFS.

Tissue processing for histological and biochemical experiments

Following the end of behavioural tests, male and female mice (in a proportion of 50% for each sex) were anaesthetized with 2,2,2-tribromethanol. Brains were removed and dissected: the anterior part from bregma 5.345 to bregma −1.355 was fixed by immersion in 4% paraformaldehyde/PBS. The caudal part was dissected into two parts along the sagittal midline. One portion was frozen, stored at −80°C and used for western blot and amyloid-β analysis, and the second was fixed in 4% paraformaldehyde/PBS.

For the biodistribution analysis, wild-type mice were sacrificed at 15 min, 1, 3, 6, 16, 24 and 48 h after the beginning of the intranasal administration. The blood was collected and the brains were dissected in olfactory bulb, cerebral cortex, hippocampus, and cerebellum. Trigeminal ganglia were also collected. The blood was processed to obtain serum by centrifugation at 10 000rpm for 10 min at 4°C. All samples were stored at −80°C until analysis. A standard curve containing brain extract and blood samples from untreated mice was used as a control, according to Malerba *et al.* (2015).

Amyloid-β_{40} and amyloid-β_{42} ELISA

To determine the levels of soluble and insoluble amyloid-β_{40} and amyloid-β_{42} brain samples were homogenized in four volumes of PBS containing a cocktail of protease inhibitors (Roche), briefly sonicated and aliquoted in two parts. One aliquot was supplemented with guanidine HCl to a final concentration of 5 M and serially diluted with ELISA sample buffer. Protein concentrations were determined using the Bradford method (Bio-Rad). Sample duplicates were then run on amyloid-β_{40} and amyloid-β_{42} colorimetric ELISAs following the protocol of the manufacturer (Life Science Technology, #KHB3441 and #KHB3482). Optical densities at 450 nm of each well were read on a Bio-Rad plate reader. Amyloid-β_{40} and amyloid-β_{42} concentrations were determined by comparison with the appropriate standard curves. All readings were in the linear range of the assay. Finally, concentration values were normalized to total brain protein concentrations and expressed in nanograms of amyloid-β per milligram total protein.

Immunoblot analysis

For western blot analysis, brains were lysed according to the fractionation method described by Sherman and Lesne (2011) and processed as described in the online Supplementary material.

Histological and neurostereological analysis

Brains were processed for immunohistochemical analysis as previously described (Capsoni *et al.*, 2000, 2002*a*) with the addition of an incubation in 50% formic acid in PBS for 30 min at room temperature performed before the preincubation step to unmask amyloid-β. Supplementary Table 4 lists primary, secondary antibodies and methods of detection.

The total number of ChAT-positive neurons in the basal forebrain (medial septum plus diagonal band) and NBM and cholinergic fibres in the cortex were calculated according to Ruberti *et al.* (2000), with the optical fraction method.

Confocal images were acquired using the TCS SL laser-scanning confocal microscope (Leica Microsystems) equipped with galvanometric stage using a 20× or a 63×/1.4 NA HCX PL APO oil immersion objective. Confocal microscope images were analysed as follows: co-localization of the different markers was analysed using the Pearson's index calculated using the Just Another Colocalisation Plugin (JACoP) of the IMAGEJ program.

Astrocytes and microglia morphology was analysed using the Filament tools of the BitPlane Imaris software.

Measurement of inflammatory markers

Simultaneous detection of multiple cytokines was obtained using a mouse inflammation antibody array (RayBiotech). Briefly, brain samples were homogenized in RIPA buffer (50 mM Tris/HCl, 150 mM NaCl, 1 mM EDTA, 1% Igepal®, 0.5% sodium deoxycholate, 0.1% SDS, protease cocktail inhibitor) and protein content determined using the Bradford method. Antibody arrays were incubated for 2 h at room temperature with blocking buffer. Five hundred micrograms of protein extract were diluted in blocking buffer and incubated with the array overnight at 4°C. Then, antibody arrays were washed according to the manufacturer's instructions and incubated for 3 h at room temperature with the biotinylated antibody cocktail solution. After washing, arrays were incubated with HRP-streptavidin for 2 h and developed using the detection buffer. Images were captured using the ChemiDoc™ detection system (Bio-Rad).

Cell cultures

To obtain astrocyte and microglia primary cell cultures, brains were collected from postnatal Day 4 B6129 mouse pups. Details are provided in the Supplementary material.

Statistical analysis

All data are reported as mean ± SEM and were calculated using the SigmaStat program v.3.5. For electrophysiological analysis, statistical comparisons were performed by two-way repeated-measures ANOVA followed by pairwise multiple-comparison procedures (Holm–Sidak method). For biochemical and histological analysis, statistical comparisons were performed by one-way ANOVA followed by pairwise *post hoc* analysis (Bonferroni method). Differences were considered significant when $P < 0.05$.

Data and materials availability

The hNGFp sequence has been deposited under the GenBank accession n. KX548900.

Results

Lack of efficacy of intraparenchymal human painless NGF

To address the question whether the local intraparenchymal delivery of NGF to the NBM decreases amyloid-β plaque load we locally delivered hNGFp close to the NBM of 3-month-old 5xFAD mice (Fig. 1A), mimicking current NGF clinical trials. We found that hNGFp caused cholinergic sprouting in the ipsilateral NBM (Fig. 1B and C) but no decrease of the amyloid-β plaque load in the cerebral cortex (Fig. 1B and D). This shows that the local delivery close to NBM is not sufficient for hNGFp to exert an anti-amyloidogenic effect, despite a clear action on cholinergic neurons and suggests that a more widespread distribution of hNGFp in the brain may be required to rescue amyloid-β deposition.

Biodistribution of human painless NGF in brain areas

To investigate whether a broader exposure of the brain to hNGFp might be more effective, we delivered hNGFp intranasally (Thorne and Frey, 2001; Malerba *et al.*, 2011). We first studied the biodistribution of hNGFp after intranasal delivery. We exploited an ELISA protocol that selectively detects the P61S tagging mutation, thus allowing the specific detection of hNGFp versus endogenous NGF (Supplementary Fig. 1A) (Covaceuszach *et al.*, 2009; Malerba *et al.*, 2015). After a single intranasal administration, hNGFp was first found in the olfactory bulb and in the trigeminal ganglion (Fig. 2A). Six and 24 h later, hNGFp was detected in the hippocampus, cerebral cortex and cerebellum, in amounts ranging from 0.5 to 1 ng/mg protein (Fig. 2A). No hNGFp could be detected in the blood serum at any time point (Fig. 2A). These results indicate that, after intranasal administration, hNGFp widely distributes to brain areas relevant to the neuropathology, such as the cerebral cortex and hippocampus, while its systemic levels are below the detection threshold. hNGFp has a wider therapeutic window than NGF, due to its higher threshold to induce pain (Capsoni *et al.*, 2012; Malerba *et al.*, 2015). Thus, the intranasal delivery route, together with the use of hNGFp, should allow delivering higher concentrations of the neurotrophin to maximize a broad exposure of the brain, while minimizing the potentially painful consequences of systemic build-up.

Establishment of the therapeutic and safe dose in 5xFAD mice

A dose-finding study was performed, by measuring memory deficits and hyperalgesia in the same 5xFAD mice. A pilot behavioural study showed that 0.54 µg/kg of intranasal hNGFp determines a full rescue of memory deficits in

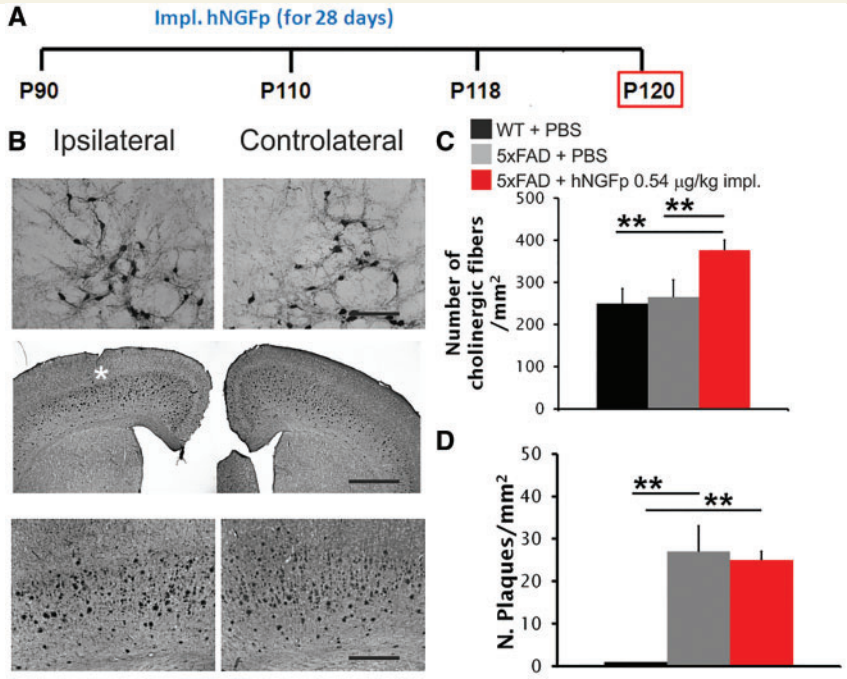

Figure 1 Local delivery of hNGFp to NBM does not decrease amyloid-β plaque load in 5xFAD mice. (**A**) Scheme of intraparenchymal delivery local to 5xFAD mice. (**B**) Immunohistochemistry for choline acetyl transferase (ChAT) in the NBM and amyloid-β in cerebral cortex of 5xFAD mice after intraparenchymal delivery of hNGFp. The white asterisk corresponds to the site of minipump implantation. (**C**) Quantification of cholinergic sprouting in NBM. (**D**) Amyloid-β plaque load in cerebral cortex, after intraparenchymal delivery of hNGFp. Scale bars are representative of mean ± SD. $n = 4$ per group, one-way ANOVA, Bonferroni *post hoc* test for pairwise comparison. Scale bars in **B** *top*, *middle* and *bottom* = 150, 500 and 200 µm, respectively. WT = wild-type. $^{**}P < 0.01$.

5xFAD mice (Fig. 2). We sought therefore to determine the maximum tolerated dose (MTD) of intranasally delivered hNGFp that would determine the rescue of the memory deficits in 5xFAD mice while not triggering pain sensitization in the orofacial region, in comparison to hNGF. Wild-type mice were treated intranasally with a single escalating dose of hNGF or hNGFp, and orofacial mechanical hyperalgesia was measured (Cha *et al.*, 2012). While hNGF induces hyperalgesia in the dose range between 0.54 and 5.4 µg/kg (Fig. 2B and C), an algesic response after hNGFp treatment was only observed for the higher doses of 2.7 and 5.4 µg/kg (Fig. 2B and C). Subsequently, hNGFp, in the dose range between 0.27 and 1.08 µg/kg, was administered daily for 3 weeks to 5xFAD mice and orofacial hyperalgesia was measured after the first and the last administration (Fig. 2D). In the dose range tested, hyperalgesia was not observed after the first administration (Fig. 2B and E) while, after 3 weeks of administration, the dose of 1.08 µg/kg started to induce sensitization (Fig. 2E). Thus, the doses between 0.27 to 0.54 µg/kg could be safely administered chronically to 5xFAD mice without inducing pain. We could also demonstrate the absence of peripheral sensitization, at the dose of 0.54 µg/kg, by measuring mechanical allodynia (Fig. 2F). To assess pharmacological effectiveness, we measured memory deficits in the same 5xFAD mice in which hyperalgesia was measured. We found that, while 0.54 and 1.08 µg/kg hNGFp were effective in rescuing spatial memory deficits, the dose of 0.27 µg/kg was not sufficient (Fig. 2F and Supplementary Fig. 1B). Thus, we concluded that hNGFp has an improved safety window with respect to wild-type hNGF and that the therapeutic and safe dose in 5xFAD mice is 0.54 µg/kg.

Rescue of synaptic plasticity deficits by human painless NGF in the entorhinal cortex of 5xFAD mice

We next verified whether the observed memory deficits in 5xFAD mice are linked to synaptic plasticity deficits in the entorhinal cortex and whether hNGFp may rescue them. Acute delivery of hNGFp to 5xFAD entorhinal cortex slices induced a rescue of the impaired long-term potentiation, which was partially inhibited by the TrkA inhibitor K252a (Supplementary Fig. 1C). To study long-term actions of hNGFp on entorhinal cortex synaptic plasticity, long-term potentiation was measured in slices from 3-month-old 5xFAD mice treated for 3 weeks with intranasal hNGFp, followed by a 1-week washout, to minimize acute effects from the last dosing (Fig. 2D). Short-term plasticity was not significantly different between wild-type and 5xFAD mice and was not influenced by hNGFp treatment

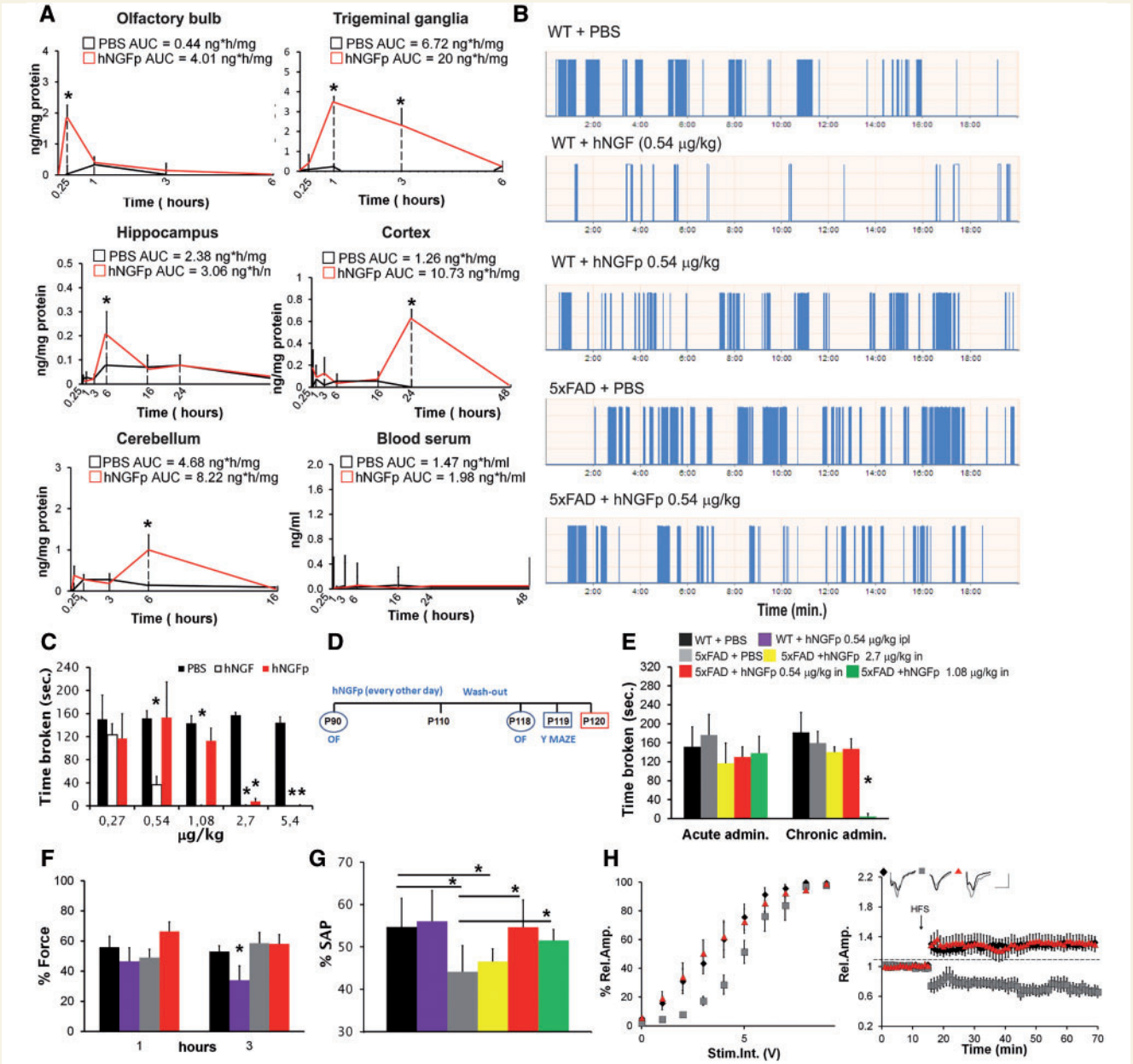

Figure 2 hNGFp distributes to brain areas relevant to Alzheimer's disease and promotes recovery from spatial memory and synaptic plasticity deficits, without triggering hyperalgesia. (**A**) Biodistribution of hNGFp in brain regions of wild-type (WT) mice after intranasal administration (n = 10 per group and time point). (**B**) Examples of output traces during the orofacial test. Each bar is a feeding event of the mouse. (**C**) Orofacial test to detect mechanical allodynia in the nose region after acute administration of hNGF or mutant hNGFp to wild-type mice (n = 10 per group). (**D**) Scheme of treatment. (**E**) Orofacial test after hNGFp administration to 5xFAD mice (n = 10 per group except mice treated with the doses of 0.27 and 1.08 µg/kg, n = 8). (**F**) Dynamic plantar aesthesiometer. (**G**) Y-maze test (n = 10 per group except mice treated with the doses of 0.27 and 1.08 µg/kg, n = 8) (**H**) Electrophysiological analysis of synaptic transmission (*left*, n = 5 slices per group), and long term potentiation (*right*) in the entorhinal cortex. Scale bars = 0.5 mV, 10 ms (n = 7 per group with the exception of wild-type mice, n = 11). Bars are representative of mean ± SD. AUC = area under the curve. $^{*}P < 0.05$.

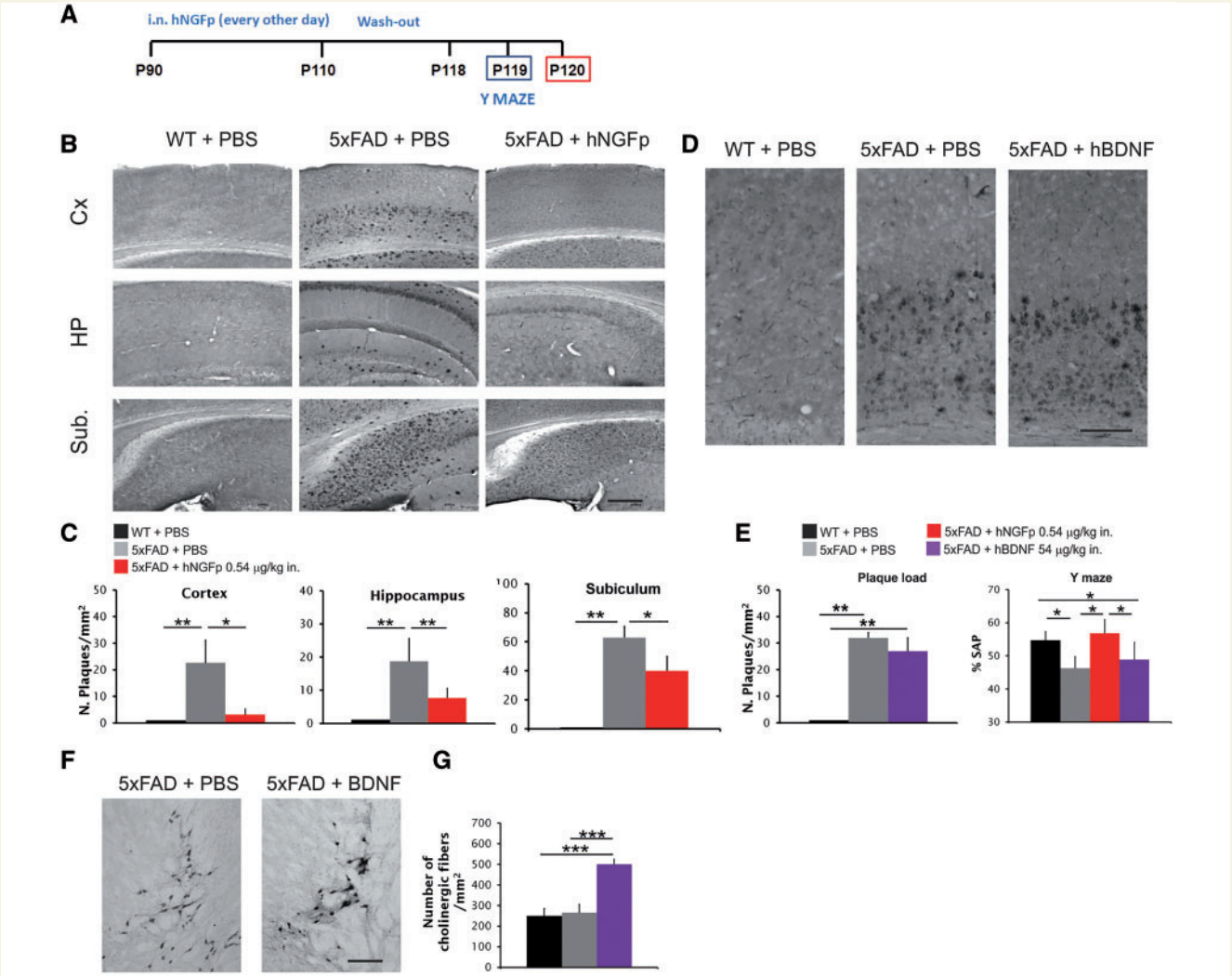

Figure 3 Intranasal hNGFp, but not BDNF, decreases amyloid-β plaque load in 5xFAD mice. (**A**) Scheme of intranasal delivery to 5xFAD mice. (**B**) Immunohistochemistry for amyloid-β in cerebral cortex, hippocampus and subiculum and (**C**) amyloid-β plaque load in cerebral cortex (Cx), hippocampus (HP) and subiculum (Sub.) after intranasal delivery of hNGFp. Scale bars are representative of mean ± SD (n = 8 per group). (**D**) Immunohistochemistry for amyloid-β in cerebral cortex after BDNF treatment. (**E**) Amyloid-β plaque load in the cortex after BDNF treatment (*left*) and Y-maze test (*right*) after BDNF intranasal treatment (n = 6 per group). (**F** and **G**) Sprouting of cholinergic fibres in the NBM after intranasal treatment with BDNF. Scale bars in **B** = 200 μm; **D** = 150 μm; **F** = 100 μm. Scale bars are representative of mean ± SD. WT = wild-type. $^{*}P < 0.05$; $^{**}P < 0.001$; $^{***}P < 0.0001$.

(Supplementary Fig. 1D and E). Synaptic strength and long-term potentiation were significantly reduced in 5xFAD mice and fully rescued by hNGFp treatment (Fig. 2H).

Decrease of amyloid-β plaque load after intranasal delivery of human painless NGF but not of BDNF

We then verified the efficacy of hNGFp in modulating the massive amyloid pathology in 3-month-old 5xFAD mice, after 3 weeks of intranasal treatment and 1 week washout (Fig. 3A). A surprisingly robust decrease of plaque load in different brain areas was observed (Fig. 3B and C and Supplementary Fig. 1F and G), as well as a general decrease of soluble and insoluble amyloid-β_{42} and amyloid-β_{40} (Supplementary Fig. 1H). To test the specificity of hNGFp action, we intranasally administered to 5xFAD mice increasing doses of BDNF, a therapeutic candidate for Alzheimer's disease (Nagahara and Tuszynski, 2011). We found that BDNF doses from 0.48 up to 54 μg/kg failed to induce a recovery of neurodegeneration. Indeed, even the higher 54 μg/kg dose did not determine a rescue of amyloid-β plaque load (Fig. 3D and E) nor of memory deficits (Fig. 3E), despite a robust sprouting of cholinergic fibres in the NBM (Fig. 3F and G), indicating that BDNF is reaching the brain targets. We concluded that hNGFp has potent anti-amyloidogenic actions that are not shared by another

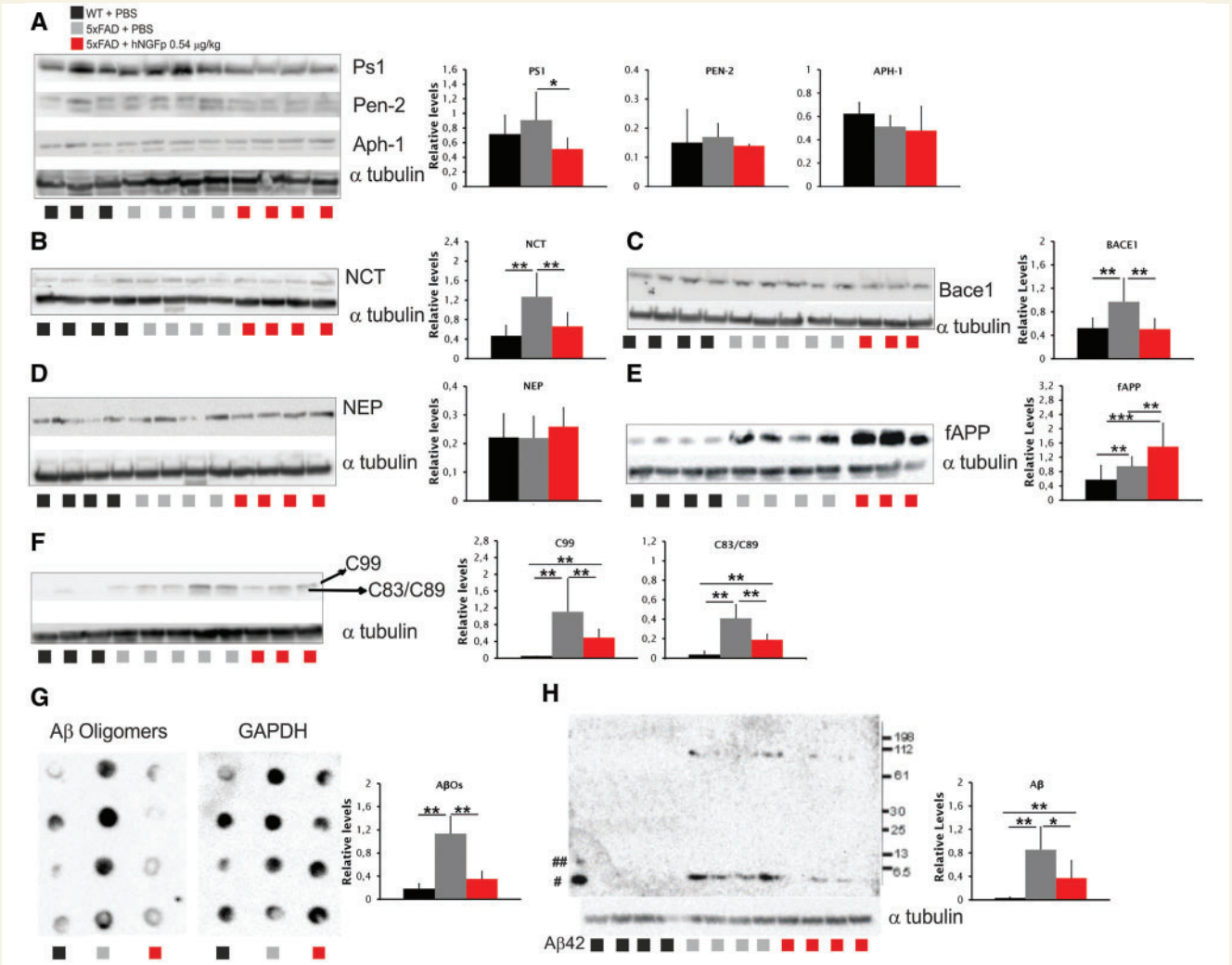

Figure 4 hNGFp promotes a reduction of pro-amyloidogenic APP processing. (**A–F** and **H**) Western blots of (**A**) PS1, anterior pharynx 1 a (APh1) and Pen-2, (**B**) nicastrin (NCT), (**C**) BACE1, (**D**) neprilysin (NEP), (**E**) full-length APP (fAPP), (**F**) c-terminal fragments, and (**H**) insoluble amyloid-β. Blots are representative of three separate experiments carried out in quadruplicate. #Monomer and ##dimer of amyloid-β are indicated. (**G**) Dot blot to detect amyloid-β oligomers. Blot is representative of two separate experiments carried out in quadruplicate. All values are given as the mean ± SD. Aβ = amyloid-β; WT = wild-type. $^{*}P < 0.05$; $^{**}P < 0.001$; $^{***}P < 0.0001$.

neuroprotective neurotrophin and that the intranasal delivery of hNGFp is much more effective than its local administration in determining a robust decrease of amyloid-β deposition. Thus, a more widespread action of hNGFp in the brain is required to achieve a pharmacological effect.

Reduction of amyloidogenic APP processing after intranasal human painless NGF

Having established that hNGFp very effectively decreases amyloid-β levels and deposition, we asked whether the expression of proteins involved in the processing of APP, such as BACE1 and proteins of the γ-secretase complex, might be modulated by hNGFp treatment. We found a significant decrease in the expression of presenilin 1 (Fig. 4A), nicastrin (Fig. 4B) and BACE1 (Fig. 4C). Interestingly, the expression of human APP and human PS1 mRNA and protein were unchanged (Supplementary Table 1 and Supplementary Fig. 2A), showing that the observed PS1 decrease is due to a decrease of mouse PS1. Increased levels of neprilysin, although not statistically significant, were also observed (Fig. 4D). The expression of anterior pharinx 1 and presenilin enhancer 2 was unaffected by hNGFp (Fig. 4A). Consistently with a reduced processing of APP, we found increased levels of full-length APP (Fig. 4E) and reduced amounts of C99 and C83/C89 terminal fragments of APP (Fig. 4F). The decrease in C83/C89 fragment did not correspond to an increased expression of ADAM 10, ADAM 17 or sAPPα (Supplementary Table 1 and Supplementary Fig. 2B and C), in line with the observed decrease of mouse BACE1. These findings correlate well with a robust decrease in the levels of amyloid-β

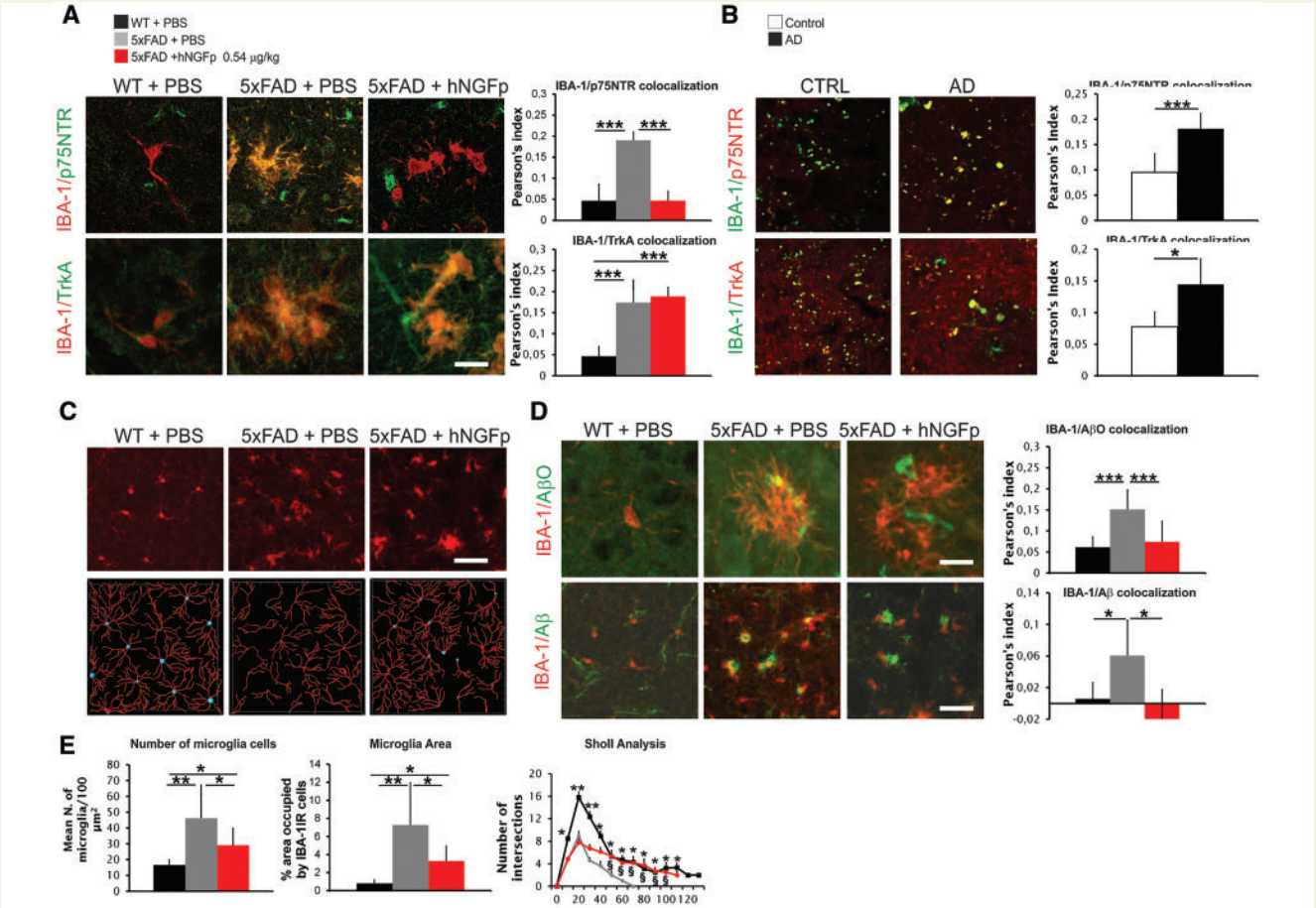

Figure 5 p75NTR and TrKA receptors are upregulated on 5xFAD microglia similarly to human Alzheimer's disease brains and their expression is modulated by hNGFp. hNGFp restores microglia morphology and amyloid-β levels. (**A**) Confocal images and co-localization analysis showing the expression of p75NTR and TrkA on microglia cells (n = 8, with the exception for hNGFp-treated mice n = 6). (**B**) Confocal images and co-localization analysis showing the expression of p75NTR and TrkA on human Alzheimer's disease (AD) microglia (n = 3). (**C**) Confocal images to detect IBA-1 and (**D**) confocal images and co-localization showing IBA-1, amyloid-β oligomers (AβO) and amyloid-β in microglia. n = 7 cells per group with exception of PBS-treated 5xFAD mice (n = 12). (**E**) Quantification of microglia number, field area occupied by microglia, and ramifications (wild-type mice n = 71 cells; PBS-treated 5xFAD mice n = 99 and hNGFp-treated 5xFAD mice n = 61). Scale bars are representative of mean ± SD. Scale bars in **A** and **D** = 10 μm; **B** = 20 μm; **C** = 60 μm. WT = wild-type. $^{*}P < 0.05$; $^{**}P < 0.001$; $^{***}P < 0.0001$.

oligomers (Fig. 4G) and of aggregated guanidinium-soluble amyloid-β (Fig. 4H). We concluded that the reduced plaque load after intranasal hNGFp administration is caused, at least in part, by a reduction of the pro-amyloidogenic APP processing.

Modulation of microglia and astrocyte morphology and activity by human painless NGF

What is the cellular basis of the anti-amyloidogenic actions of hNGFp in 5xFAD mice? In these mice, amyloid-β is produced mainly by cortical neurons (Supplementary Fig. 3A), which do not express TrkA receptors (Supplementary Fig. 3B). Hence, these neurons cannot be the first targets of the potent anti-amyloidogenic action of hNGFp. We considered unlikely that activation of BFCNs by hNGFp is sufficient to induce the potent anti-amyloidogenic response observed (Fig. 1). Thus, we hypothesized that the cells mediating hNGFp action might be microglia and/or astrocytes, which are potential target cells for NGF (De Simone *et al.*, 2007; Cragnolini *et al.*, 2009, 2012).

In cortical microglia of wild-type mice, both p75NTR and total TrkA were undetectable *in vivo* (Fig. 5A and Supplementary Fig. 4A and B), while they were readily detectable in cultured wild-type primary microglia (Supplementary Fig. 4C). Both receptors were instead well expressed in the cortex of PBS-treated 5xFAD mice (Fig. 5A and Supplementary Fig. 4A and B). Interestingly, a similar increase in p75NTR and TrkA microglia expression could be observed in brain sections from Alzheimer's disease patients (Fig. 5B).

After hNGFp treatment, p75NTR immunoreactivity in 5xFAD cortical microglia was decreased, while TrkA

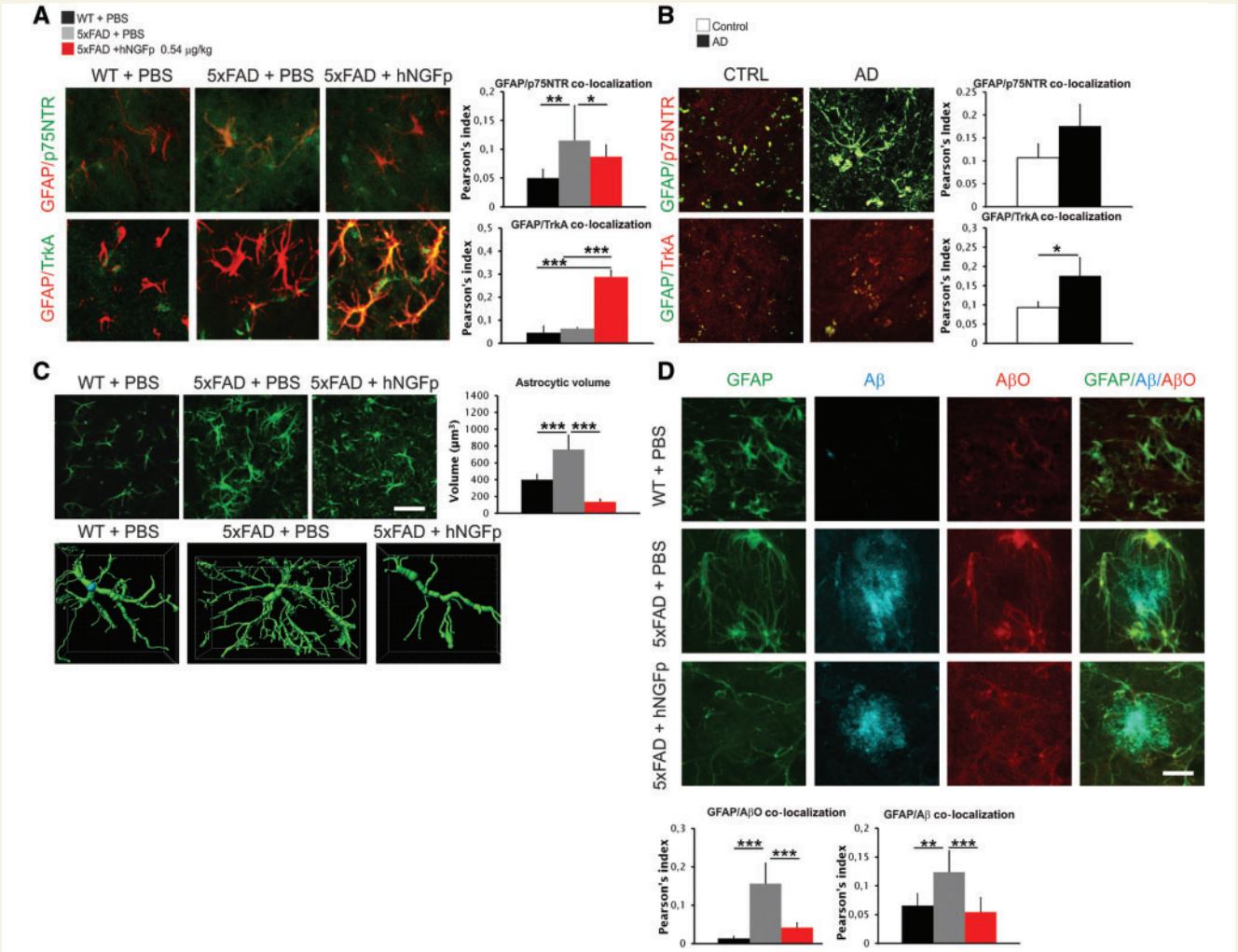

Figure 6 p75NTR and TrKA receptors are upregulated on 5xFAD astrocytes similarly to human Alzheimer's disease brains and their expression is modulated by hNGFp. hNGFp restores astrocyte morphology and amyloid-β species levels. (**A**) Confocal images and co-localization analysis showing the expression of p75NTR and TrkA on astrocytes cells (n = 5 with the exception for wild-type mice n = 8). (**B**) Confocal images and co-localization analysis showing the expression of p75NTR and TrkA on human Alzheimer's disease (AD) astrocytes (n = 3). (**C**) Confocal images to detect GFAP and quantification of astrocytic volume (n = 20 cells per group). (**D**) Confocal images and co-localization showing GFAP, amyloid-β oligomers (AβO) and amyloid-β in astrocytes (n = 10 cells per group). Scale bars are representative of mean ± SD. Scale bars in **A** and **D** = 15 μm; **B** = 20 μm; **C** = 60 μm. CTRL = control; WT = wild-type. $^{*}P < 0.05$; $^{**}P < 0.001$; $^{***}P < 0.0001$.

immunoreactivity remained high (Fig. 5A and Supplementary Fig. 4A and B).

5xFAD mice showed a higher number of large microglial cells, characterized by a lower number of ramifications, with respect to wild-type mice (Fig. 5C and E). hNGFp decreased the number and the size of microglia cells and partially restored their morphological complexity (Fig. 5C and E). 5xFAD microglia cells are engulfed by different amyloid-β species (Fig. 5D and Supplementary Fig. 4D and E). hNGFp induced a robust decrease of both amyloid-β and amyloid-β oligomer immunoreactivity (Fig. 5D and Supplementary Fig. 4D and E).

Cortical astrocytes from wild-type mice, similarly to microglia, do not express p75NTR and TrkA at detectable levels *in vivo* (Fig. 6A), but do so in culture (Supplementary Fig. 5A). A significantly increased astrocytic p75NTR immunoreactivity was found in PBS-treated 5xFAD mice, which was decreased after hNGFp treatment (Fig. 6A and Supplementary Fig. 5B). TrkA immunoreactivity in astrocytes was undetectable both in wild-type and PBS-treated 5xFAD mice, but a robust increase in astrocytic TrkA was observed after hNGFp administration (Fig. 6A and Supplementary Fig. 5C). Most importantly, also in Alzheimer's disease brain sections, we could detect an increased expression of both p75NTR and TrkA in astrocytes (Fig. 6B).

As for astrocyte morphology, 5xFAD mice showed extensive astrogliosis, characterized by an increase in the

volume of individual astrocytes (Fig. 6C), which was reduced after hNGFp treatment (Fig. 6C). In addition, similarly to microglia, the treatment with hNGFp decreased amyloid-β and amyloid-β oligomer immunoreactivity in 5xFAD astrocytes (Fig. 6D).

hNGFp is a preferential TrkA binder, with respect to p75NTR (Covaceuszach *et al.*, 2010). hNGFp shifts the expression of NGF receptors towards TrkA on both cell types. Since, in PBS-treated 5xFAD mice, TrkA is expressed primarily on microglia and not in astrocytes (Supplementary Table 2), we postulated that microglia represent the primary target of hNGFp action and that astrocytes may represent a secondary target. In any event, an increased degradation of cellular amyloid-β forms taken up by microglia and astrocytes may significantly contribute to the overall reduction of amyloid-β deposition after hNGFp treatment.

The chemokine CXCL12 is a mediator of human painless NGF actions

To investigate the mechanism whereby hNGFp determines the rescue of amyloid-β deposition and memory deficits we hypothesized that hNGFp might modulate the expression of microglia-derived cytokines and chemokines. A cytokine and chemokine profiling revealed that hNGFp treatment increases the levels of the soluble TNFα receptor II (sTNFRII) (an extracellular decoy of TNFα), of macrophage inflammatory protein 1α and 1γ (MIP-1α and MIP-1γ) and of CXCL12 (also known as SDF-1α) (Fig. 7A and B, and Supplementary Table 3). We focused on CXCL12, which has been shown to modulate amyloid-β expression (Parachikova and Cotman, 2007; Laske *et al.*, 2008*a*, *b*). Surprisingly, we found that CXCL12 expression was not upregulated in microglia (Fig. 7C) but in neurons (Fig. 7D). Thus, we searched for a factor that could modulate CXCL12 expression in neurons. One candidate is TNFα, as its levels are known to be regulated by NGF (Marshall *et al.*, 1999; Prencipe *et al.*, 2014). It is known that CXCL12 can be upregulated by low TNFα (Zhang *et al.*, 2008; Bockstal *et al.*, 2011) in non-neuronal cells and, consistently, we show that the incubation of wild-type and 5xFAD cultured cortical neurons with TNFα decreases CXCL12 expression, providing a link between TNF signalling and neuronal CXCL12 (Supplementary Fig. 6A). hNGFp treatment reduced the expression of TNFα in 5xFAD microglia (Supplementary Fig. 6B). Likewise, hNGFp reduced TNFα expression in wild-type microglia cultures, treated with amyloid-β oligomers (Supplementary Fig. 6C). Contrary to microglia, we found an increased TNFα immunoreactivity in cortical astrocytes of hNGFp-treated 5xFAD (Supplementary Fig. 6D). The opposite regulation of TNFα by hNGFp in 5xFAD microglia versus astrocytes results in the observed overall unchanged levels of TNFα in 5xFAD whole brain extracts (Supplementary Table 2). However, the observed overall increase of the extracellular TNFα decoy sTNFRII, after hNGFp treatment (Fig. 7A and B and Supplementary Table 3), together with the microglia-specific hNGFp-induced reduction of TNFα, point to the reduction of microglia-derived TNFα signalling as the mechanism whereby hNGFp treatment increases neuronal CXCL12 expression.

We tested the hypothesis that CXCL12 may mediate the rescuing effects of hNGFp on memory deficits and on amyloidogenic APP processing. 5xFAD mice were therefore co-treated with hNGFp and AMD3100 (Fig. 8A), an inhibitor of CXCL12 receptor CXCR4, which is expressed on neurons, astrocytes and microglia (Guyon, 2014). The treatment of 5xFAD mice with AMD3100 completely counteracted the rescuing effects of hNGFp on memory deficits (Fig. 8B), on amyloid-β plaque load (Fig. 8C and Supplementary Fig. 7A) and on the levels of amyloid-β oligomers (Fig. 8D and Supplementary Fig. 7B). AMD3100 also blocks the hNGFp-induced modulation of presenilin 1 (Fig. 8E and Supplementary Fig. 7C), BACE1 (Fig. 8F and Supplementary Fig. 7C) and of APP processing products (Fig. 8G–I and Supplementary Fig. 7C). The co-treatment with AMD3100 completely blocked the reduction of intracellular amyloid-β induced by hNGFp in microglia cells but not the decrease of intracellular amyloid-β oligomers (Fig. 8J and Supplementary Fig. 8A and B). AMD3100 also counteracted the induction of TrkA expression in astrocytes *in vivo* by hNGFp and the consequent decrease of amyloid-β oligomers but had no effect on the decrease of amyloid-β species (Fig. 8K and Supplementary Fig. 8C and D).

These data demonstrate that CXCL12 mediates most of the actions of intranasally delivered hNGFp in 5xFAD mice.

In keeping with this conclusion, CXCL12 also decreased amyloid-β oligomer immunoreactivity in 5xFAD cultured cortical neurons (Supplementary Fig. 9A) and protected wild-type neurons from cell death induced by incubation with 7PA2 amyloid-β oligomers (Walsh *et al.*, 2002) (Supplementary Fig. 9B). Moreover, either hNGFp or CXCL12 similarly counteracted the marked decrease of phospho-TrkA induced by amyloid-β oligomers in cultured cortical astrocytes from wild-type mice (Supplementary Fig. 9C).

In conclusion, hNGFp exerts its neuroprotective actions in 5xFAD mice via microglia and astrocytes, which in neurodegenerative conditions express TrkA (Fig. 8L), thereby lowering the overall TNFα signalling and inducing neuronal CXCL12. This chemokine is an obligatory mediator of the neuroprotective and anti-amyloidogenic actions of hNGFp in 5xFAD mice.

Discussion

The clinical use of NGF as a therapeutic agent for Alzheimer's disease has a strong rationale that goes beyond its actions on BFCNs (Mufson *et al.*, 1999;

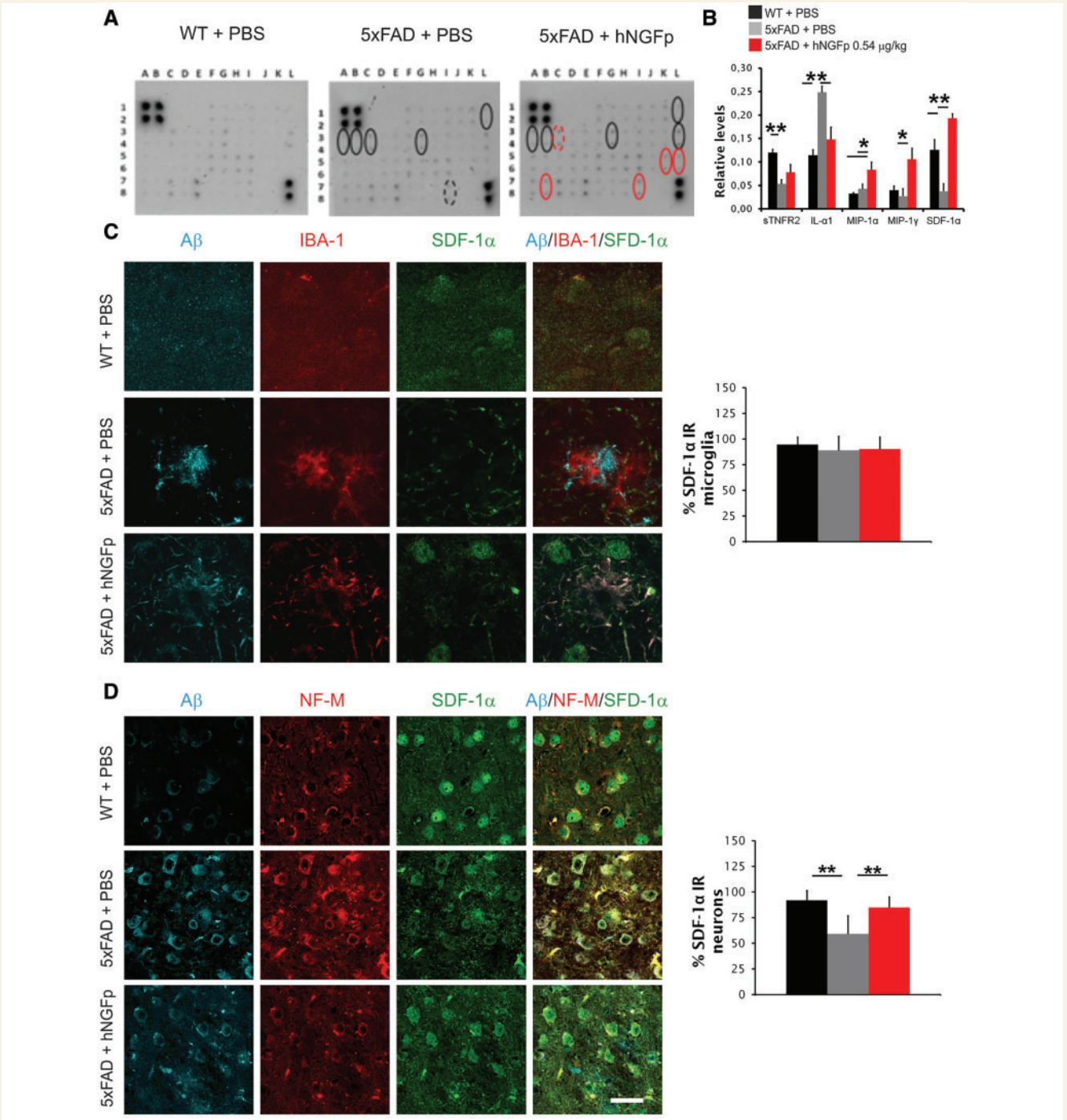

Figure 7 hNGFp modulates the expression of inflammatory cytokines in brain extracts. CXCL12 is increased in neuronal cells. (**A**) Immunoblot and (**B**) quantification to detect inflammatory cytokines in brain extracts. Scale bars are representative of mean ± SD ($n = 4$ per group). Details are provided in Supplementary Table 2. (**C**) Confocal images and co-localization analysis showing the expression of amyloid-β, IBA-1 and CXCL12 in microglia. (**D**) Confocal images and co-localization analysis showing the expression of amyloid-β, NF-M and CXCL12 in neurons. Scale bars are representative of mean + SD ($n = 9$ with the exception for hNGFp-treated mice $n = 6$). Scale bars in **A** = 15 μm; **C** and **D** = 32.5 μm. WT = wild-type. $^{*}P < 0.05$; $^{**}P < 0.001$.

Capsoni and Cattaneo, 2006; Capsoni *et al.*, 2011; Cattaneo and Calissano, 2012), but is hampered by its potent pain sensitizing activity, forcing current clinical trials in Alzheimer's disease patients to an invasive intraparenchymal delivery (Tuszynski *et al.*, 2005; Eriksdotter-Jonhagen *et al.*, 2012). To facilitate the therapeutic uses of NGF, we designed the mutant hNGFp, which has identical neurotrophic properties to hNGF, but a significantly lower pain-sensitizing activity (Capsoni *et al.*, 2012; Malerba *et al.*, 2015). Here we demonstrated the remarkable efficacy

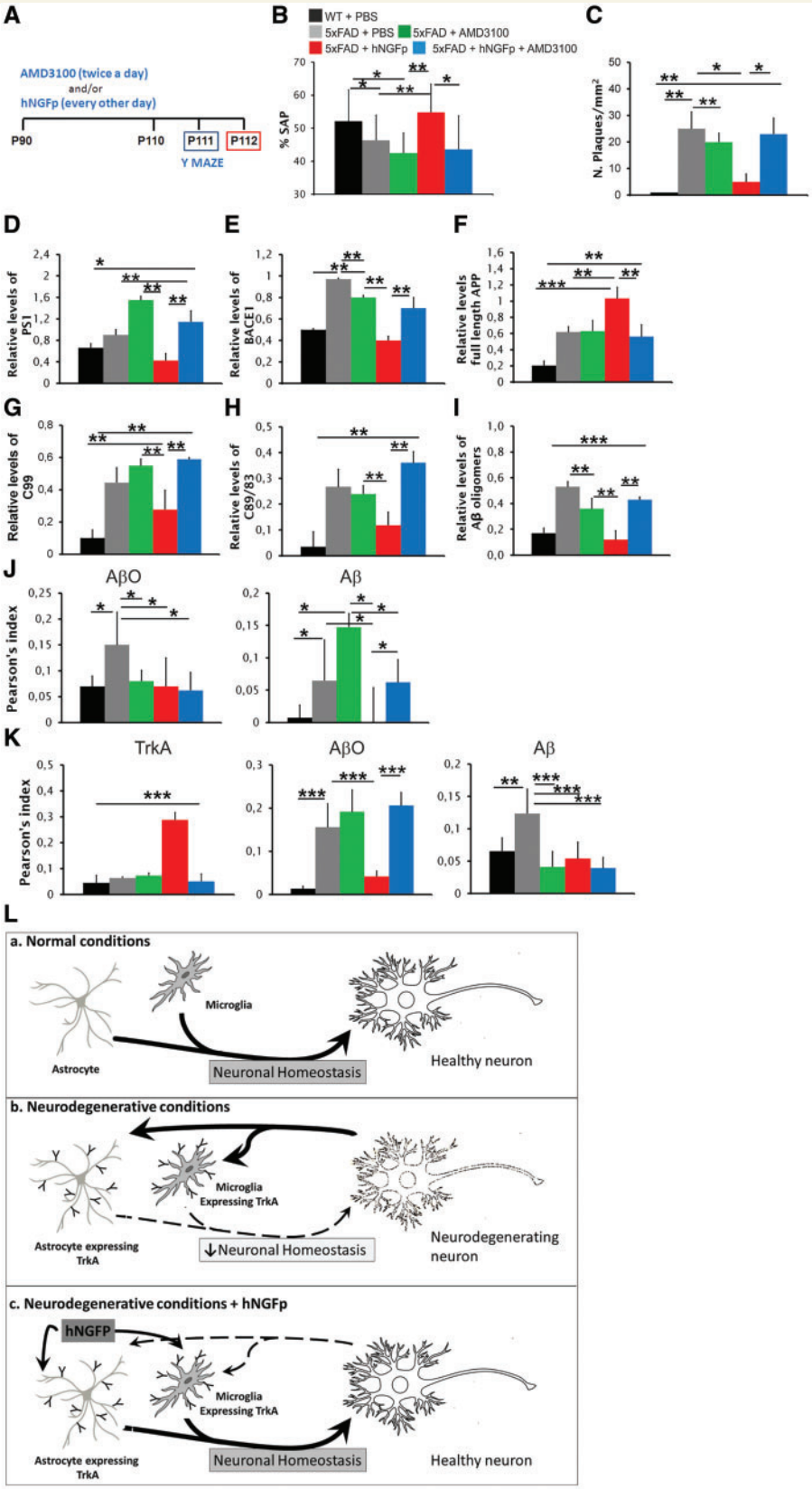

Figure 8 Co-administration of hNGFp with the CXCR4 inhibitor AMD3100 prevents the recovery of memory deficits, the decrease in APP processing, the amyloid-β species decrease in microglia and astrocytes, and the increase of TrkA astrocyte expression induced by intranasal hNGFp. (**A**) Scheme of the treatment with intranasal hNGFp and AMD3100; (**B**) Y maze test; and (**C**) amyloid-β plaque load in cerebral cortex (n = 10 per group). Quantification of western blots for (**D**) presenilin 1, (**E**) BACE 1, (**F**) full-length APP and (**G** and **H**) CTFs. (**I**) Quantification of dot blot to detect amyloid-β oligomers. (**J**) Co-localization of amyloid-β species and amyloid-β

(continued)

of intranasally delivered hNGFp in counteracting neurodegeneration and behavioural deficits in the aggressive mouse model 5xFAD (Oakley *et al.,* 2006), starting the treatment at an age (postnatal Day 90) when the pathology is already well evident, similar to a prospective clinical situation. On the other hand, a continuous local intraparenchymal delivery of hNGFp, close to the NBM, mimicking current NGF clinical trials (Tuszynski *et al.,* 2005; Mandel, 2010; Eriksdotter-Jonhagen *et al.,* 2012; Ferreira *et al;* 2015; Karami *et al.,* 2015), failed to rescue neurodegeneration, despite a clear sprouting of BFCNs. This suggests that the neuroprotective actions of hNGFp cannot be mediated by the cholinergic system, also because, at this age, 5xFAD mice have no cholinergic deficit (Supplementary Fig. 10). The potent neuroprotective and anti-amyloidogenic actions of hNGFp in this model require therefore a global biodistribution of hNGFp in relevant brain regions, such as that obtained by intranasal delivery. The fact that hNGFp takes 6 h or more to reach regions such as hippocampus and cortex is not surprising, and in agreement with published data on the intracellular transport of WGA-HRP (wheat germ agglutinin-horseradish peroxidase) or other biologics such as insulin growth factor-1 (Lochhead and Thorne, 2012). This has important implications for the design of future NGF-based clinical trials. Systemic leakage of hNGFp after intranasal delivery is low, so that hNGFp does not induce peripheral mechanical allodynia, also due to its higher pain-inducing threshold. A dose-response study, in which orofacial pain and spatial memory were jointly measured, allowed finding a safe effective dose without pain induction. The anti-neurodegenerative action of hNGFp is highly specific, since it is not exerted by the related neurotrophin BDNF (not even at a 100-fold higher dose than hNGFp), strengthening the conclusion that the broad neuroprotective action of hNGFp is not mediated by BFCNs, which respond to both NGF and BDNF (Hefti *et al.*, 1993; Mufson *et al.*, 1999). The question arises as to what is the cellular basis for the observed actions of hNGFp. We demonstrate that microglia and astrocytes mediate hNGFp actions. In 5xFAD brain, both microglia and astrocytes express TrkA and p75NTR receptors with a p75NTR/TrkA ratio in favour of p75NTR. This imbalance is changed by hNGFp, which shifts the expression of NGF receptors towards TrkA on both cell types. Previous studies have shown that microglia take up both soluble and insoluble forms of amyloid-β *in vitro* and *in vivo* (Bolmont *et al.*, 2008; Lee and Landreth, 2010) but also that phagocytosis may not be effective in compensating the continuous deposition of amyloid-β (Bolmont *et al.*, 2008; Sierra *et al.*, 2013). Similarly, astrocytes have been shown to take up amyloid-β *in vitro* and *in vivo* (Wyss-Coray *et al.*, 2003) with a feed-forward mechanism driven by cytokines and amyloid-β_{42}, eventually leading to amyloid-β production also in these cells (Zhao *et al.*, 2011). The dramatic overall reduction of amyloid-β deposition after hNGFp is carried out, at least partially, by a reduced APP amyloidogenic processing and, also, by an increased degradation of cellular amyloid-β forms taken up by microglia and astrocytes. The observed increase in the TNFα decoy sTNFαRII, together with the observed increase of TNFα in microglia cells, should lead to a reduced TNFα signalling by microglia, which is expected to upregulate the neuronal expression of the chemokine CXCL12 (Zhang *et al.*, 2008; Bockstal *et al.*, 2011 and this study). Indeed, we found a neuron-selective increase of CXCL12, which has well established neuroprotective (Guyon and Nahon, 2007; Li *et al.*, 2012) and anti-amyloidogenic actions (Parachikova and Cotman, 2007; Laske *et al.*, 2008*a*, *b*). Most importantly, CXCL12 is downregulated in Alzheimer's disease brains (Parachikova and Cotman, 2007; Laske *et al.*, 2008*a*, *b*). We tested the hypothesis that CXCL12 may mediate the neuroprotective actions of hNGFp and, by exploiting the AMD3100 inhibitor of the CXCL12 receptor CXCR4, provided compelling evidence that CXCL12 mediates the pharmacological effects of hNGFp in 5xFAD mice.

Based on these data, we can draw a picture whereby hNGFp would act primarily on microglia and astrocytes in the neurodegenerating brain, leading to a decreased availability of TNFα to neurons that, possibly with other undefined factors, in turn mediate an increase of neuronal CXCL12 levels and the downstream reduction of APP processing and broad neuroprotection and restoration of neuron-to-glia homeostasis (Fig. 8L).

In summary, we provide evidence that a 3-week pharmacological treatment with hNGFp, using the clinically feasible intranasal administration, promotes the recovery of synaptic and behavioural deficits and amyloid-β-linked neurodegeneration, in a mouse model affected by a dramatic production and deposition of this peptide. It is noteworthy that the treatment was initiated after the pathology was well established. These data add a strong mechanistic rationale to the clinical uses of hNGFp in neurodegenerative diseases, by validating microglia and astrocytes as cellular

Figure 8 Continued

oligomers in microglia. (**K**) Co-localization of TrkA, amyloid-β species (detected using mAb 4G8) and amyloid-β oligomers (detected using ScFv A13) in astrocytes. Scale bars are representative of mean ± SD; $n = 10$ per group in each analysis. (**L**) General mechanism of action of intranasal hNGFp. (**a**) In normal conditions, microglia and astrocytes do not express TrkA receptors and contribute to maintain neuronal homeostasis. (**b**) In neurodegenerative conditions, glial cells start to express TrkA as a protective reaction to neurodegeneration, which is (**c**) boosted by the intranasal administration of hNGFp. AβO = amyloid-β oligomers. $^{*}P < 0.05$; $^{**}P < 0.001$; $^{***}P < 0.0001$.

targets for its strong neuroprotective actions. Notably, we established that glial cells mediate the rescuing effect by hNGFp, via the CXCL12 chemokine, identifying a new anti-neurodegenerative pathway that may become a target for new therapeutic opportunities for Alzheimer's disease and other neurodegenerative diseases.

Acknowledgements

The authors are grateful to Matteo Caleo (Institute of Neuroscience, National Council for Research, Pisa, Italy) for advice and discussions, to Marta Pietrasanta (Bio@SNS, Laboratory of Biology, Scuola Normale Superiore, Pisa, Italy) for technical assistance in setting up the mini osmotic pumps implantation and to Prof. Dennis Selkoe (Harvard Medical School USA) for providing the 7PA2 cell line.

Funding

This work has been partially supported by the Alzheimer Drug Discovery Foundation (ADDF) grant n. 20120601, The Italian Ministry of Higher Education and Scientific Research (FIRB n. RBAP10L8TY) and Fondazione Roma. These supporting sources had no involvement in the study design, collection, analysis or interpretation of data, nor were they involved in writing the paper or in the decision to submit this report for publication.

Supplementary material

Supplementary material is available at *Brain* online.

References

Anderson WW, Collingridge GL. The LTP Program: a data acquisition program for on-line analysis of long-term potentiation and other synaptic events. J Neurosci Methods 2001; 108: 71–83.

Bartus RT, Dean RL, 3rd, Beer B, Lippa AS. The cholinergic hypothesis of geriatric memory dysfunction. Science 1982; 217: 408–14.

Bockstal V, Geurts N, Magez S. Acute disruption of bone marrow B lymphopoiesis and apoptosis of transitional and marginal zone B cells in the spleen following a blood-stage plasmodium chabaudi infection in mice. J Parasitol Res 2011; 2011: 534697.

Bolmont T, Haiss F, Eicke D, Radde R, Mathis CA, Klunk WE, et al. Dynamics of the microglial/amyloid interaction indicate a role in plaque maintenance. J Neurosci 2008; 28: 4283–92.

Capsoni S, Brandi R, Arisi I, D'Onofrio M, Cattaneo A. A dual mechanism linking NGF/proNGF imbalance and early inflammation to Alzheimer's disease neurodegeneration in the AD11 anti-NGF mouse model. CNS Neurol Disord Drug Targets 2011; 10: 635–47.

Capsoni S, Cattaneo A. On the molecular basis linking Nerve Growth Factor (NGF) to Alzheimer's disease. Cell Mol Neurobiol 2006; 26: 619–33.

Capsoni S, Covaceuszach S, Ugolini G, Spirito F, Vignone D, Stefanini B, et al. Delivery of NGF to the brain: intranasal versus ocular administration in anti-NGF transgenic mice. J Alzheimers Dis 2009; 16: 371–88.

Capsoni S, Giannotta S, Cattaneo A. Beta-amyloid plaques in a model for sporadic Alzheimer's disease based on transgenic anti-nerve growth factor antibodies. Mol Cell Neurosci 2002a; 21: 15–28.

Capsoni S, Giannotta S, Cattaneo A. Nerve growth factor and galantamine ameliorate early signs of neurodegeneration in anti-nerve growth factor mice. Proc Natl Acad Sci USA 2002b; 99: 12432–7.

Capsoni S, Marinelli S, Ceci M, Vignone D, Amato G, Malerba F, et al. Intranasal "painless" human nerve growth factor slows amyloid neurodegeneration and prevents memory deficits in app X PS1 mice. PLoS One 2012; 7: e37555.

Capsoni S, Ugolini G, Comparini A, Ruberti F, Berardi N, Cattaneo A. Alzheimer-like neurodegeneration in aged antinerve growth factor transgenic mice. Proc Natl Acad Sci USA 2000; 97: 6826–31.

Cattaneo A, Calissano P. Nerve growth factor and Alzheimer's disease: new facts for an old hypothesis. Mol Neurobiol 2012; 46: 588–604.

Cattaneo A, Capsoni S, Paoletti F. Towards non invasive Nerve Growth Factor therapies for Alzheimer's disease. J Alzheimers Dis 2008; 15: 255–83.

Cha M, Kohan KJ, Zuo X, Ling JX, Gu JG. Assessment of chronic trigeminal neuropathic pain by the orofacial operant test in rats. Behav Brain Res 2012; 234: 82–90.

Covaceuszach S, Capsoni S, Marinelli S, Pavone F, Ceci M, Ugolini G, et al. In vitro receptor binding properties of a "painless" NGF mutein, linked to hereditary sensory autonomic neuropathy type V. Biochem Biophys Res Commun 2010; 391: 824–9.

Covaceuszach S, Capsoni S, Ugolini G, Spirito F, Vignone D, Cattaneo A. Development of a non invasive NGF-based therapy for Alzheimer's disease. Curr Alzheimer Res 2009; 6: 158–70.

Cragnolini AB, Huang Y, Gokina P, Friedman WJ. Nerve growth factor attenuates proliferation of astrocytes via the p75 neurotrophin receptor. Glia 2009; 57: 1386–92.

Cragnolini AB, Volosin M, Huang Y, Friedman WJ. Nerve growth factor induces cell cycle arrest of astrocytes. Dev Neurobiol 2012; 72: 766–76.

De Rosa R, Garcia AA, Braschi C, Capsoni S, Maffei L, Berardi N, et al. Intranasal administration of nerve growth factor (NGF) rescues recognition memory deficits in AD11 anti-NGF transgenic mice. Proc Natl Acad Sci USA 2005; 102: 3811–6.

De Simone R, Ambrosini E, Carnevale D, Ajmone-Cat MA, Minghetti L. NGF promotes microglial migration through the activation of its high affinity receptor: modulation by TGF-beta. J Neuroimmunol 2007; 190: 53–60.

Einarsdottir E, Carlsson A, Minde J, Toolanen G, Svensson O, Solders G, et al. A mutation in the nerve growth factor beta gene (NGFB) causes loss of pain perception. Hum Mol Genet 2004; 13: 799–805.

Eriksdotter-Jonhagen M, Linderoth B, Lind G, Aladellie L, Almkvist O, Andreasen N, et al. Encapsulated cell biodelivery of nerve growth factor to the Basal forebrain in patients with Alzheimer's disease. Dement Geriatr Cogn Disord 2012; 33: 18–28.

Ferreira D, Westman E, Eyjolfsdottir H, Almqvist P, Lind G, Linderoth B, et al. Brain changes in Alzheimer's disease patients with implanted encapsulated cells releasing nerve growth factor. J Alzheimers Dis 2015; 43: 1059–72.

Frey IW, Liu J, Chen XQ, Thorne RG, Fawcett JR, Ala TA, et al. Delivery of ^{125}I-NGF to the brain via the olfactory route. Drug Deliv 1997; 4: 87–92.

Guyon A. CXCL12 chemokine and its receptors as major players in the interactions between immune and nervous systems. Front Cell Neurosci 2014; 8: 65.

Guyon A, Nahon JL. Multiple actions of the chemokine stromal cell-derived factor-1alpha on neuronal activity. J Mol Endocrinol 2007; 38: 365–76.

Hefti F, Knusel B, Lapchak PA. Protective effects of nerve growth factor and brain-derived neurotrophic factor on basal forebrain cholinergic neurons in adult rats with partial fimbrial transections. Prog Brain Res 1993; 98: 257–63.

Karami A, Eyjolfsdottir H, Vijayaraghavan S, Lind G, Almqvist P, Kadir A, et al. Changes in CSF cholinergic biomarkers in response

to cell therapy with NGF in patients with Alzheimer's disease. Alzheimers Dement 2015; 11: 1316–28.
Kimura R, Devi L, Ohno M. Partial reduction of BACE1 improves synaptic plasticity, recent and remote memories in Alzheimer's disease transgenic mice. J Neurochem 2010; 113: 248–61.
Laske C, Stellos K, Eschweiler GW, Leyhe T, Gawaz M. Decreased CXCL12 (SDF-1) plasma levels in early Alzheimer's disease: a contribution to a deficient hematopoietic brain support? J Alzheimers Dis 2008a; 15: 83–95.
Laske C, Stellos K, Stransky E, Seizer P, Akcay O, Eschweiler GW, et al. Decreased plasma and cerebrospinal fluid levels of stem cell factor in patients with early Alzheimer's disease. J Alzheimers Dis 2008b; 15: 451–60.
Lee CY, Landreth GE. The role of microglia in amyloid clearance from the AD brain. J Neural Transm 2010; 117: 949–60.
Levi-Montalcini R. Effects of mouse tumor transplantation on the nervous system. Ann N Y Acad Sci 1952; 55: 330–44.
Levi-Montalcini R, Skaper SD, Dal Toso R, Petrelli L, Leon A. Nerve growth factor: from neurotrophin to neurokine. Trends Neurosci 1996; 19: 514–20.
Li M, Hale JS, Rich JN, Ransohoff RM, Lathia JD. Chemokine CXCL12 in neurodegenerative diseases: an SOS signal for stem cell-based repair. Trends Neurosci 2012; 35: 619–28.
Lochhead JJ, Thorne RG. Intranasal delivery of biologics to the central nervous system. Adv Drug Deliv Rev 2012; 64: 614–28.
Malcangio M, Ramer MS, Boucher TJ, McMahon SB. Intrathecally injected neurotrophins and the release of substance P from the rat isolated spinal cord. Eur J Neurosci 2000; 12: 139–44.
Malerba F, Paoletti F, Bruni Ercole B, Materazzi S, Nassini R, Coppi E, et al. Functional Characterization of Human ProNGF and NGF Mutants: Identification of NGF P61SR100E as a "Painless" Lead Investigational Candidate for Therapeutic Applications. PLoS One 2015; 10: e0136425.
Malerba F, Paoletti F, Capsoni S, Cattaneo A. Intranasal delivery of therapeutic proteins for neurological diseases. Expert Opin Drug Deliv 2011; 8: 1277–96.
Mandel RJ. CERE-110, an adeno-associated virus-based gene delivery vector expressing human nerve growth factor for the treatment of Alzheimer's disease. Curr Opin Mol Ther 2010; 12: 240–7.
Marshall JS, Gomi K, Blennerhassett MG, Bienenstock J. Nerve growth factor modifies the expression of inflammatory cytokines by mast cells via a prostanoid-dependent mechanism. J Immunol 1999; 162: 4271–6.
Maurice T, Su TP, Privat A. Sigma1 (sigma 1) receptor agonists and neurosteroids attenuate B25-35-amyloid peptide-induced amnesia in mice through a common mechanism. Neuroscience 1998; 83: 413–28.
Mufson EJ, Kroin JS, Sendera TJ, Sobreviela T. Distribution and retrograde transport of trophic factors in the central nervous system: functional implications for the treatment of neurodegenerative diseases. Prog Neurobiol 1999; 57: 451–84.
Nagahara AH, Tuszynski MH. Potential therapeutic uses of BDNF in neurological and psychiatric disorders. Nat Rev Drug Discov 2011; 10: 209–19.
Oakley H, Cole SL, Logan S, Maus E, Shao P, Craft J, et al. Intraneuronal beta-amyloid aggregates, neurodegeneration, and neuron loss in transgenic mice with five familial Alzheimer's disease mutations: potential factors in amyloid plaque formation. J Neurosci 2006; 26: 10129–40.
Origlia N, Righi M, Capsoni S, Cattaneo A, Fang F, Stern DM, et al. Receptor for advanced glycation end product-dependent activation of p38 mitogen-activated protein kinase contributes to amyloid-beta-mediated cortical synaptic dysfunction. J Neurosci 2008; 28: 3521–30.
Parachikova A, Cotman CW. Reduced CXCL12/CXCR4 results in impaired learning and is downregulated in a mouse model of Alzheimer disease. Neurobiol Dis 2007; 28: 143–53.
Pesavento E, Capsoni S, Domenici L, Cattaneo A. Acute cholinergic rescue of synaptic plasticity in the neurodegenerating cortex of anti-nerve-growth-factor mice. Eur J Neurosci 2002; 15: 1030–6.
Petty BG, Cornblath DR, Adornato BT, Chaudhry V, Flexner C, Wachsman M, et al. The effect of systemically administered recombinant human nerve growth factor in healthy human subjects. Ann Neurol 1994; 36: 244–6.
Poduslo JF, Curran GL. Permeability at the blood-brain and blood-nerve barriers of the neurotrophic factors: NGF, CNTF, NT-3, BDNF. Brain Res Mol Brain Res 1996; 36: 280–6.
Prencipe G, Minnone G, Strippoli R, De Pasquale L, Petrini S, Caiello I, et al. Nerve growth factor downregulates inflammatory response in human monocytes through TrkA. J Immunol 2014; 192: 3345–54.
Ruberti F, Capsoni S, Comparini A, Di Daniel E, Franzot J, Gonfloni S, et al. Phenotypic knockout of nerve growth factor in adult transgenic mice reveals severe deficits in basal forebrain cholinergic neurons, cell death in the spleen, and skeletal muscle dystrophy. J Neurosci 2000; 20: 2589–601.
Sherman MA, Lesne SE. Detecting abeta*56 oligomers in brain tissues. Methods Mol Biol 2011; 670: 45–56.
Sierra A, Abiega O, Shahraz A, Neumann H. Janus-faced microglia: beneficial and detrimental consequences of microglial phagocytosis. Front Cell Neurosci 2013; 7: 6.
Thorne RG, Frey WH, 2nd. Delivery of neurotrophic factors to the central nervous system: pharmacokinetic considerations. Clin Pharmacokinet 2001; 40: 907–46.
Tuszynski MH, Smith DE, Roberts J, McKay H, Mufson E. Targeted intraparenchymal delivery of human NGF by gene transfer to the primate basal forebrain for 3 months does not accelerate beta-amyloid plaque deposition. Exp Neurol 1998; 154: 573–82.
Tuszynski MH, Thal L, Pay M, Salmon DP, U HS, Bakay R, et al. A phase 1 clinical trial of nerve growth factor gene therapy for Alzheimer disease. Nat Med 2005; 11: 551–5.
Walsh DM, Klyubin I, Fadeeva JV, Cullen WK, Anwyl R, Wolfe MS, et al. Naturally secreted oligomers of amyloid beta protein potently inhibit hippocampal long-term potentiation *in vivo*. Nature 2002; 416: 535–9.
Whitehouse PJ, Price DL, Struble RG, Clark AW, Coyle JT, Delon MR. Alzheimer's disease and senile dementia: loss of neurons in the basal forebrain. Science 1982; 215: 1237–9.
Wyss-Coray T, Loike JD, Brionne TC, Lu E, Anankov R, Yan F, et al. Adult mouse astrocytes degrade amyloid-beta in vitro and in situ. Nat Med 2003; 9: 453–7.
Zhang Q, Guo R, Schwarz EM, Boyce BF, Xing L. TNF inhibits production of stromal cell-derived factor 1 by bone stromal cells and increases osteoclast precursor mobilization from bone marrow to peripheral blood. Arthritis Res Ther 2008; 10: R37.
Zhao J, O'Connor T, Vassar R. The contribution of activated astrocytes to Abeta production: implications for Alzheimer's disease pathogenesis. J Neuroinflamm 2011; 8: 150.